

Properties of argon adlayers deposited on graphite from Monte Carlo calculations

E. Flenner and R. D. Etters

Physics Department, Colorado State University, Fort Collins, Colorado 80523, USA

(Received 14 November 2005; published 21 March 2006)

Properties of argon adlayers deposited on a graphite substrate are calculated using a high resolution Monte Carlo calculation. Nine different surface densities are examined ranging from very partial to slightly beyond a complete monolayer. At low densities the calculated specific heats show two peaks. One is very sharp and one is broad. The sharp peak is shown to signal on orientational transition of the adlayer, and the broad one signals melting. The melting curve is calculated and compared with experiments, as are the lattice parameters at various temperatures. It is shown that second layer promotion plays an important role in the behavior of adlayers at some densities and temperatures. The orientational angle of the adlayer, with respect to the sublattice, is determined at various temperatures, and it is argued that the rotational transition is due to the relaxation of stress on the adlayer. It is found that the rotational transition disappears when the surface density increases beyond about 84% of that of a complete monolayer. This is in accord with experimental evidence. In order to identify and characterize the features of adlayers, various order parameters and probability distributions are calculated.

DOI: [10.1103/PhysRevB.73.125419](https://doi.org/10.1103/PhysRevB.73.125419)

PACS number(s): 68.43.-h, 64.70.Dv

I. INTRODUCTION

The behavior of argon adlayers deposited on a graphite substrate has been a robust area of inquiry for three decades, and experimental results have shown that this system is complicated. The objective of this calculation is to resolve many of the remaining questions about Ar/Gr and integrate that information into a general understanding of quasi-two-dimensional adlayers.

The early specific heat measurements of Chang¹ on Ar/Gr showed a single broad melting peak centered at about 50 K for surface densities $n \leq 0.84$. These units are such that n is unity for a complete monolayer. At $n=0.97$, the peak was at 78.5 K. The author concluded that the results were entirely consistent with a continuous melting transition. The later high resolution specific heat measurements of Migone, Li, and Chan² showed an additional feature not seen in the work of Chang. For surface densities $\rho \leq 1.043$, a sharp narrow peak was observed at temperatures about two Kelvin below the broad peak at 49.5 K. Its full width at half maximum (FWHM) is 0.3 K. Here the surface density ρ is given in units of $\rho_0 = 0.0636$ atoms/ \AA^2 , which is also the density of the $\sqrt{3} \times \sqrt{3}$ commensurate structure. These units will be used in this work. For comparison, the complete monolayer density for the incommensurate Ar/Gr system is $\rho \approx 1.25$. Migone *et al.*² identified the sharp peak as evidence for a “weakly first order” melting transition and the broad peak was vaguely explained as a gradual loss of the sixfold symmetry of the solid. In a more recent work, Ma *et al.*³ repeated the specific heat measurements of Migone *et al.*² at $\rho=0.4$. The results were the same as reported previously. They also identified the sharp peak as a first order melting transition. When they added even a small fraction of CH₄ or Xe impurities, the sharp peak disappeared and the broad peak remained.

Scattering experiments⁴⁻⁸ have contributed much information about the Ar/Gr system. Low energy electron diffrac-

tion (LEED) results⁸ showed that the triangular structure of the argon adlayer does not lay along one of the sixfold $\sqrt{3} \times \sqrt{3}$ symmetry axes of the substrate. Instead it is rotated away by several degrees. In the x-ray measurements of D’Amico *et al.*⁷ at $\rho \approx 0.81$, it was found that the rotational angle continuously reduces from 2.87° at 44.29 K to 2° at 50.03 K. They determined that the melting temperature is at $T_m = 49.67$ K. Thus they conclude that the rotated state persists into the fluid. The synchrotron x-ray scattering of Nielsen *et al.*,⁶ at submonolayer densities, showed similar results to the other scattering experiments and they also speculated that the narrow specific heat peak may be a loss of orientational order over a narrow temperature interval. They did not determine the rotational angles. All of the scattering experiments conclude that melting is continuous and none can identify the character of the narrow or the broad specific heat peaks.

Interest in the order of two-dimensional (2D) melting has been heightened by the possibility that it is continuous, unlike 3D systems that exhibit first order transitions. A theory for the melting of strictly 2D layers was introduced by Kosterlitz, Thouless, Halperin, Nelson, and Young (KTHNY),⁹ where a continuous transition is possible. According to the theory, melting would proceed into a hexatic fluid with short range positional order and with quasi-long-range bond orientational order. Then, at a higher temperature, this hexatic fluid would undergo a second transition into an isotropic fluid. Important to that view of melting for Ar/Gr is that the KTHNY theory predicts an undetectable essential singularity in the specific heat at the first melting temperature, followed by a broad anomaly at higher temperatures. Another possible outcome of the KTHNY theory is a first order melting transition similar to 3D systems.

Nearly all 2D systems that have been examined exhibit first order melting transitions.¹⁰⁻¹³ Two possible exceptions are Xe/Gr and Ar/Gr. It is agreed that Xe/Gr is first order for submonolayers, but at higher densities the order of melting is not settled.^{5,14} It is argued that the formation of a

second layer complicates the analysis. The uncertainty in the order of melting in Ar/Gr is embodied in Refs. 2, 3, 6, and 15. There have been many computer simulations^{15–27} designed to probe the nature of Ar/Gr. These works did not exhibit any peaks in the specific heat nor was there evidence presented for bond orientation epitaxy. However, Abraham²⁶ examined the configurations generated for a partial monolayer and concluded that melting started at 47 K and continuously evolved until about 55 K. He also determined that the probability of finding an Ar atom near the center of a substrate hexagon is much higher than at other positions, despite the fact that Ar/Gr is incommensurate. Previously, he had argued²⁶ that all 2D systems exhibit a first order melting transition. Note that the minimum in the interaction between a single Ar atom and the substrate is above the center of a substrate hexagon.

A more recent Monte Carlo calculation,²⁸ at $\rho=0.71$, gave a probability distribution of Ar atoms at various points on the substrate unit cell that is in accord with the results of Abraham. Also, a large, broad peak in the specific heat was observed at 50 K, but not a second peak. A high resolution extension of this work²⁹ was conducted at $\rho=0.71$ and 0.89, where adjacent calculated points were often separated by less than 0.1 K. The calculated specific heat showed two peaks, a sharp, narrow peak at 43.8 K and a broad peak at 49.5 K. Thus, the results are in accord with the measurements of Migone *et al.*² and Ma *et al.*,³ but the interpretation was quite different. The calculation²⁹ clearly showed that the sharp, narrow peak is due to a rotational transition of the adlayer from an angle off the substrate symmetry axis to that axis. The broad peak at higher temperature was shown to be a signature of melting, which was consistent with a continuous transition. With this interpretation, the nature of melting given by the specific heat and the scattering measurements are in accord. Thus, there is agreement that Ar/Gr exhibits a continuous melting transition which no doubt will create new interest in the KTHNY theory. Also calculated was the temperature dependence of the adlayer rotational angle Θ with respect to the substrate symmetry axis. It was found that the rotational angle was constant at about 2.5° at low temperatures until the rotational transition temperature was reached, where it rapidly dropped to zero. The entire change occurred in 0.3 K. That is also approximately the full width at half maximum of the sharp specific heat peak. An x-ray diffraction measurement⁷ showed Θ changes continuously with temperature and shows no signature across the rotational transition. Moreover, it is still two degrees even into the melt. This difference between experiment and the calculation was not resolved.

This article is designed to extend the calculations described earlier and to examine the many properties not yet resolved. The system is studied at nine different surface densities in the interval $0.39 \leq \rho \leq 1.31$. This interval covers from very partial monolayers to slightly greater than monolayer densities. The melting curve is determined over that range and the peaks in the specific heat are identified. It is of particular interest to explain why the sharp peak disappears for $\rho \geq 1.05$. Lattice parameters are calculated and their thermal expansion is given. The rotational angle of the adlayer with respect to the substrate is also determined; this includes

the effect of second layer promotion. In addition, the probability distribution of adlayer atoms over the substrate is calculated. This result underscores the importance of the large variation in the adatom-substrate potential across the surface.

II. METHOD AND INTERACTIONS

Properties of the Ar/Gr system are determined from a Monte Carlo method using an (N, ρ, T) ensemble, where N is the number of argon atoms in the MC cell and T is the temperature. Most results were calculated with $N=256$, but as many as 1600 were sometimes used to guard from unwanted size effects. Thermal averages of physical quantities were formed from as many as 2×10^7 steps. Each step consists of randomly moving all $3N$ atomic coordinates. The length of the simulations for each temperature was determined as follows. First an initial run was conducted until the energy appeared to converge. Second the simulation was run until the running average of the energy and the specific heat were oscillating around an equilibrium value. Then the length of the simulation was doubled and it was verified that the average energy and the specific heat were statistically equal if they were calculated using the first half of the simulation, the second half of the simulation, and if the whole simulation was used for the calculations. Periodic boundary conditions are employed in the (x, y) plane of the substrate to simulate a macroscopic system. There are no boundary conditions in the \hat{z} direction normal to the substrate. Because the Ar adlayer is incommensurate with the substrate symmetry, the application of boundary conditions must be applied with care. One way to apply periodic boundary conditions that are the same for the MC cell and the substrate, even though they are incommensurate, is to choose surface densities for which the MC cell is an integer multiple of the substrate unit cell. This strategy is used in this work.

The potential energy of the system is given by

$$U = \sum_{i < j}^N U_{\text{Ar-Ar}}(r_{ij}) + \sum_{i < j}^N U_{\text{SM}}(\vec{r}_i, \vec{r}_j) + \sum_{i=1}^N U_{\text{Ar-Gr}}(\vec{r}_i), \quad (1)$$

where $r_{ij} = |\vec{r}_i - \vec{r}_j|$ and \vec{r}_i is the location of the i th argon atom. The potential of Aziz and Slamen³⁰ for $U_{\text{Ar-Ar}}$ is used, and it is recognized to be a highly accurate representation of the Ar-Ar pair potential. The calculated three body correction³¹ was neglected since it contributes less than 2% of the dispersion energy. The term U_{SM} represents the substrate-mediated dispersion interaction of McLachlen.³² It is a correction that comes from dipoles induced due to the proximity of the graphite substrate, and we use the parameters given by Bruch.³³ The image plane is located 1.6785 Å above the substrate plane. The term $U_{\text{Ar-Gr}}$ represents the overlap-dispersion part of the adlayer-substrate interaction, and the anisotropic form of Carlos and Cole³⁴ is used. The parameters (σ, ϵ) are from Steele.³⁵ This term is Fourier transformed with respect to the substrate symmetry, which gives an infinite series. The first two terms are sufficient. Thus,

$$U_{\text{Ar-Gr}} = E_0(z) + E_1(x, y, z). \quad (2)$$

Notice that E_0 depends only on the distance the adatoms are from the substrate and E_1 is the leading term that accounts

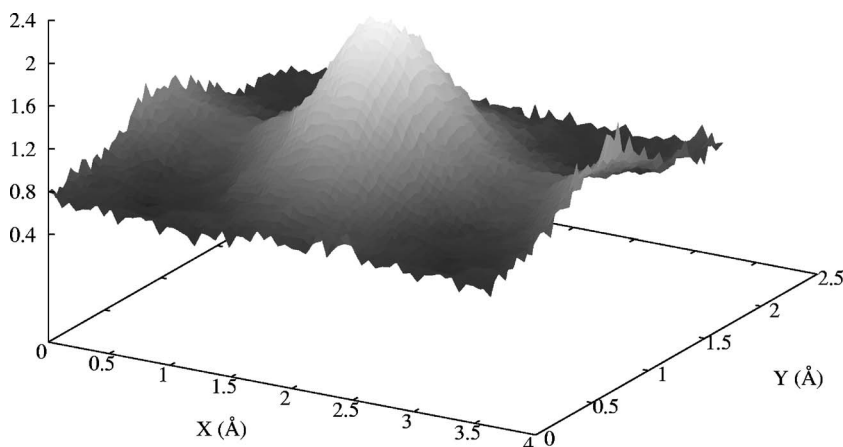


FIG. 1. The probability distribution of argon atoms over the substrate unit cell with $(\rho, T) = (0.71, 35 \text{ K})$. It is normalized to unity everywhere if there is an equal probability of finding an argon atom at any point over the unit cell. The maximum is at the center of a graphite hexagon and the minima are over the carbon atoms.

for the lateral variation in the adatom-substrate interaction. This method results in treating the graphite substrate as rigid in the simulation. The total potential (1) with the parameters cited above was used in the previous work.²⁹ It has been speculated that these parameters make the strength of the substrate mediated and the Ar-Gr potential terms too high, and there is some indirect evidence for that.³⁶ In this work we have examined the effect of varying the strength of U_{SM} and U_{Ar-Gr} well within the uncertainty just mentioned. In particular, in previous work,²⁹ the only quantitative departure with experiment was the calculated separation between the two peaks in the specific heat of $\Delta T \approx 5.8 \text{ K}$. Experiment² shows that ΔT is approximately 2 K. Using the strength of the substrate mediated and the argon-substrate terms in the total potential as parameters, a search was conducted to close the above mentioned difference in ΔT . The search was constrained to parameters that left other calculated physical quantities essentially unchanged. A reduction of the strengths of both terms by 15% achieved the desired effect, and this change is well within the known uncertainty. This work incorporates this reduction.

III. RESULTS

Many important features of the Ar/Gr system are a consequence of competition between forces between argon atoms and those between the argon atoms and the substrate. The minimum in the argon-substrate potential is over the center of the hexagon formed by six substrate carbon atoms, and the minimum in the Ar pair potential occurs at a separation of about 3.8 Å. It is easy to see from these potential parameters that the minimum energy state of the system is not an adlayer commensurate with the substrate symmetry, as experiment^{8,37} confirms. The adatom-substrate potential acts to pull the adlayer toward a commensurate $\sqrt{3} \times \sqrt{3}$ structure and the adatom-adatom potential resists that expansion.

Figure 1 shows the calculated probability distribution for finding an argon atom at various points over the graphite unit cell at $(\rho, T) = (0.71, 35 \text{ K})$. The distribution is normalized to unity, which it would be everywhere if the argon atoms have equal probability of being anywhere over the unit cell. This would also be the case if the term E_1 in Eq. (2) were neglected. Figure 1 dramatizes the importance of the modula-

tion in the substrate potential embodied in E_1 . It also shows that the probability of finding an Ar atom near the center of a substrate hexagon is quite large, as Abraham²⁶ previously noted. As the temperature approaches melting, the probability distribution becomes only slightly more flat and the modulation persists into the fluid but in a diminished way. The distribution is qualitatively the same for other surface densities.

The specific heat is calculated using the fluctuation of the internal energy. Figure 2 shows the results for $\rho = 0.39, 0.71$, and 1.00. There is a small narrow peak at around 47.3 K with a FWHM of 0.3 K, and a large broad peak at about 50 K. Note that the separation between the two peaks is close to the experimental value.² The calculated specific heat at $\rho = 1.07, 1.14, 1.22$, and 1.31 are shown in Fig. 3. They differ from those at lower densities because there is only one peak, which is quite broad. However, at the highest densities that peak becomes narrow, particularly at $\rho = 1.31$. Sections III A and III B describe the behavior of the argon adlayer around the specific heat peaks.

A. Melting

Several order parameters are used to understand the character of the specific heat. One is

$$\Psi_6 = \frac{1}{N_B} \left\langle \sum_{j,k} \exp(6i\Phi_{jk}) \right\rangle, \quad (3)$$

where Φ_{jk} is the angle a bond between two Ar atoms (j, k) have with respect to a fixed, but otherwise arbitrary axis in the (x, y) plane. The sum on j extends over all adatoms in the Monte Carlo cell and the sum on k is over all nearest neighbors of j . The brackets indicate a thermal average. The factor N_B is the number of bonds used in the calculation. This order parameter is unity if the adlayer structure exhibits six-fold symmetry, as does a triangular lattice. It is zero for an isotropic fluid. Also of interest is the susceptibility of Ψ_6 ,

$$\chi_6 = \frac{[\langle \Psi_6^2 \rangle - \langle \Psi_6 \rangle^2]}{T} \quad (4)$$

which should peak at a transition that signals the loss of sixfold symmetry. Figures 4–6 show Ψ_6 and χ_6 for $\rho = 0.39$,

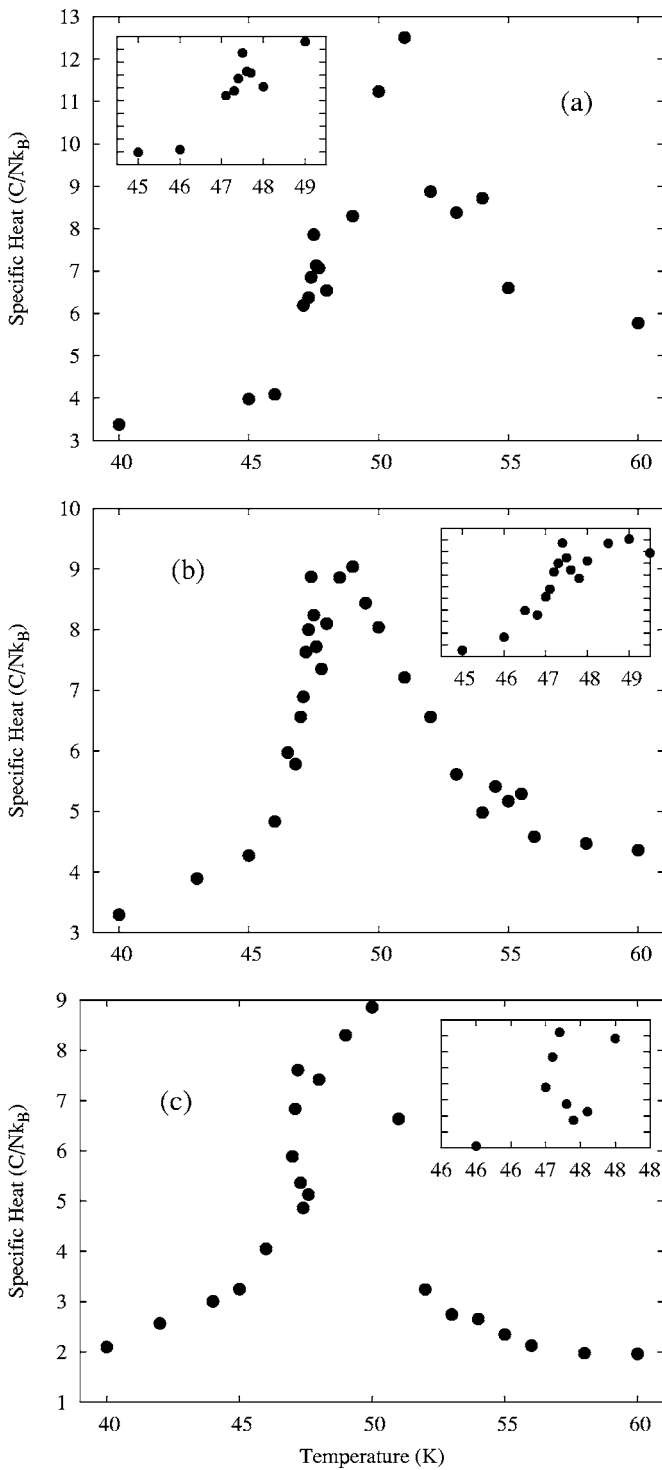


FIG. 2. The calculated specific heats at $\rho=0.39, 0.71,$ and 1.00 from top to bottom, respectively. The region of the sharp peaks are magnified in the insets. The uncertainty around the peaks is less than 7%, and the uncertainty for $T < 0.45$ and $T > 0.55$ is less than the size of the points.

1.00, and 1.22, respectively. Results for the other densities are qualitatively the same. Note that Ψ_6 drops from near unity to near zero over a temperature interval equal to the FWHM of the broad specific heat peak. Moreover, the peak in χ_6 occurs at the same temperatures as observed for the

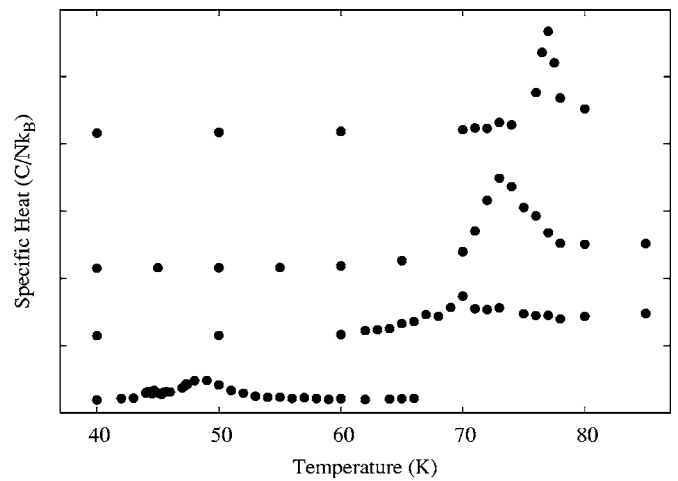


FIG. 3. The calculated specific heats for $\rho=1.07, 1.14, 1.22,$ and 1.31 listed from bottom to top. The uncertainty in the specific heat is less than 7% around the peaks and less than 1% for temperatures more than five degrees from the peak position for each density.

broad specific heat peak. Thus, the broad peak corresponds to a transition where the sixfold structural symmetry is lost. This is consistent with melting. This interpretation is supported by the calculated pair distribution and a visual examination of the configurations. Moreover, proof will be given later that the sharp peak in the specific heat is a signature of an orientational transition, not melting.

The solid circles on Fig. 7 show the calculated melting temperatures at nine different surface densities in the range $0.39 \leq \rho \leq 1.31$. The two points at densities 1.08 and 1.09 were calculated from only the order parameters. The conservative error flags reflect this additional statistical uncertainty. The other points have a statistical uncertainty of ± 0.5 K. The squares and the triangles represent the experimental results.^{1,2} Another feature of the calculated melting peaks in the specific heat at various densities is that the peak heights and their full width at half maximum are comparable to experimental results.^{1,2} For example, the peak heights are about constant for densities $\rho < 1.07$ where they reduce by more

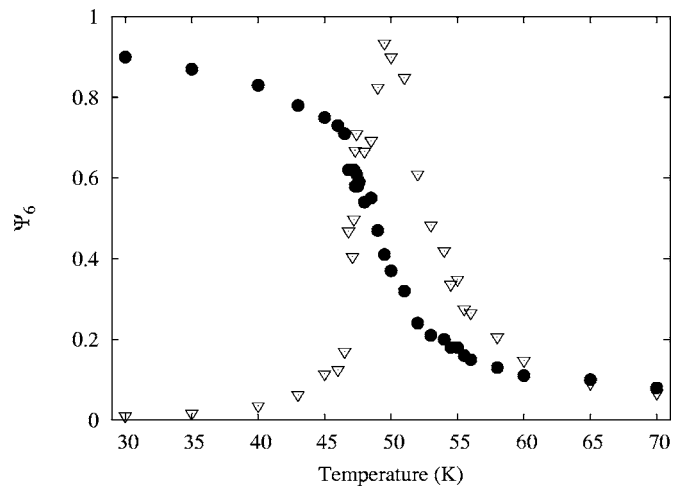


FIG. 4. The solid circles represent the order parameter Ψ_6 for $\rho=0.39$. The inverted triangles shows the susceptibility χ_6 .

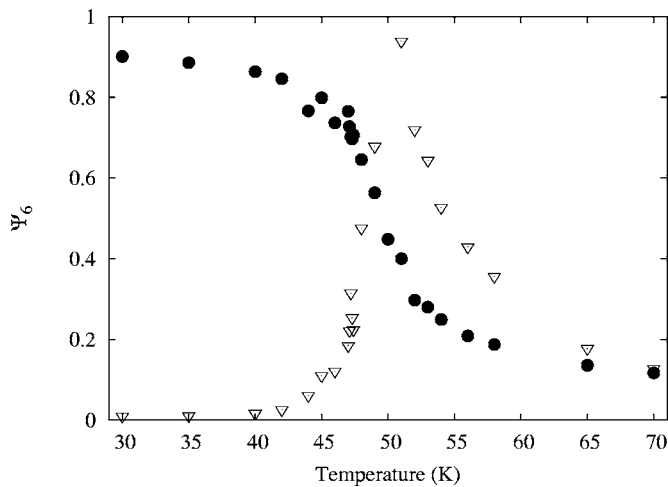


FIG. 5. The same format as Fig. 4 for $\rho=1.00$.

than half. For $\rho > 1.07$ the peak heights increase rapidly. One objective of this work was to determine if the character of the melting curve for Ar/Gr could be calculated as successfully as was done for N₂/Gr.^{38,39} Moreover, are the arguments made to explain the features of the melting curve in the previous work³⁸ valid? The answer seems to be yes, and a discussion of this will be presented later.

B. Orientational behavior of the adlayer

It remains to characterize the small, narrow specific heat peak. The narrow peak is observed experimentally² at all densities less than 1.043, and it vanishes at higher densities. This calculation shows the same feature. The peak appears for all densities up to 1.00, for the next calculated point at $\rho=1.07$, and for higher densities it vanishes. This behavior has not been previously explained. The orientational character of the adlayer provides the answer. The angle the Ar adlayer is rotated from one of the sixfold $\sqrt{3} \times \sqrt{3}$ symmetry axes of the substrate is determined by the following procedure. For each step, the angle every nearest neighbor Ar-Ar bond makes with a $\sqrt{3} \times \sqrt{3}$ symmetry axis of the substrate is

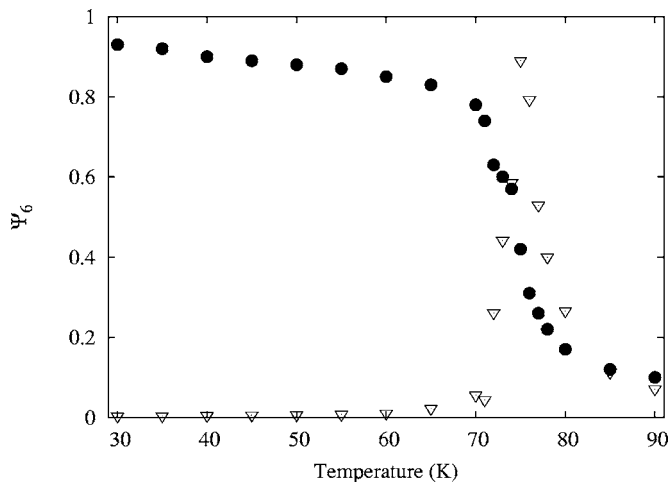


FIG. 6. The same format as Fig. 4 for $\rho=1.22$.

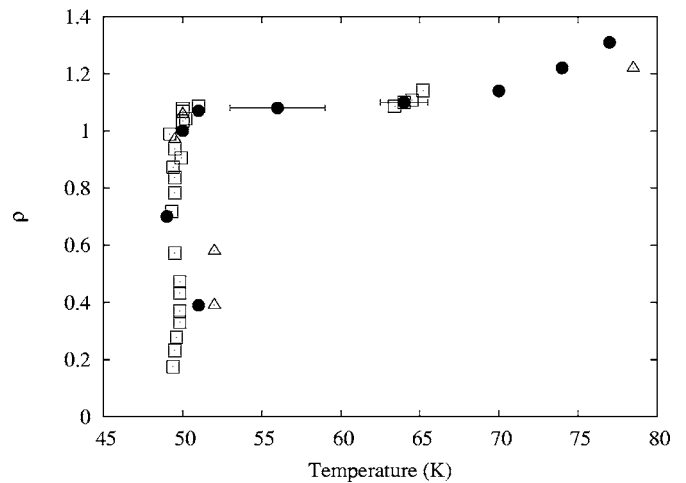


FIG. 7. The solid circles represent the calculated melting temperatures at various surface densities. That statistical uncertainty is about the size of the points, except for $\rho=1.08$ and 1.09 , where the calculations were less precise. The flags reflect the additional uncertainty. The open squares (Ref. 2) and the triangles (Ref. 1) represent the experimental results.

measured. For convenience we map them about one of the sixfold symmetry axis and an average of the rotational angle is determined. The same is done for every step used for calculating thermodynamic equilibrium quantities. From this data a probability distribution for the rotational angles is formed for each (ρ, T) . The peak in the distribution identifies the rotational angle Θ . The distribution for each of the three densities exhibiting two specific heat peaks, $\rho=0.39, 0.71$, and 1.00 are qualitatively the same. For temperatures below about 46.5 K a single, narrow peak is easily resolved with a nonzero angle Θ . In the interval $46.5 \text{ K} < \Theta < 47.2 \text{ K}$, two peaks occur at $\pm\Theta$. This is expected since the substrate symmetry demands that a rotation of Θ is equivalent to a rotation of $-\Theta$. Only one peak is observed at lower temperatures because there is a potential barrier between the two equivalent states, and the thermal energy is not sufficient to breach it in an acceptable number of MC steps. Beyond 47.2 K a broad peak appears at Θ equal zero and the peaks at $\pm\Theta \neq 0$ remain as shoulders around the broad central peak. By $T=48 \text{ K}$ only the central peak remains at $\Theta=0$. The adlayer has rotated along the substrate symmetry axis. Figure 8 shows the calculated rotational angle for $\rho=0.39, 0.71$, and 1.0 . Note that the rotational angle drops rapidly to zero at about 47.2 K, which is precisely the temperature calculated for the location of the narrow specific heat peak and reported by experiment.² Moreover, the change in Θ occurs in a temperature interval about equal to the FWHM of that peak. This is compelling evidence that this peak is associated with a rotational transition.

Additional evidence for the above assignment comes from the fourth cumulant of the rotational angle

$$C_4 = 1 - \frac{\langle \Theta^4 \rangle}{3 \langle \Theta^2 \rangle^2}. \tag{5}$$

Since rotational states at angles $(\Theta, -\Theta)$ are equivalent by symmetry, the system can be viewed as in a double well

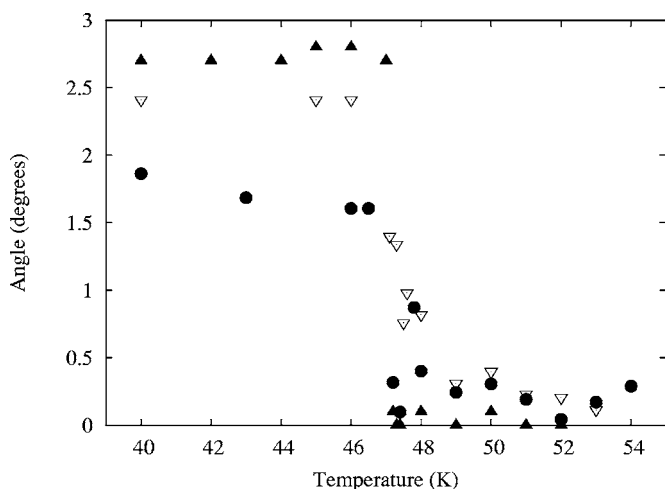


FIG. 8. The calculated rotational angles versus temperatures. The open, inverted triangles are for $\rho=0.39$, the solid triangles represent $\rho=1.00$, and the solid circles represent $\rho=0.71$.

orientational potential. It follows that the system should be well described by a two state Ising model, which is signaled by explicit expectations for C_4 . That is, C_4 must equal $2/3$ at low temperature and zero at high temperature, and $C_4 = 0.52$ at the critical point. The results in Fig. 9 show that C_4 satisfies all the above requirements and it rapidly changes between its limiting values at about 47.3 ± 0.03 K, which is at the critical point. These results are similar to those shown in Fig. 3 of a previous work.²⁹ Note that the sharp change in C_4 occurs at the same temperature calculated for the sharp specific heat peak, which is significantly lower than the melting temperature. Another signature of the orientational transition is the behavior of the potential energy term E_1 , which becomes more negative at about 47.3 K, and becomes more positive as the melting temperature is approached. Also, the lattice parameter shows a small, sharp increases at the rotational transition temperature. These features suggest that the transition occurs in an attempt to relieve the stress on the

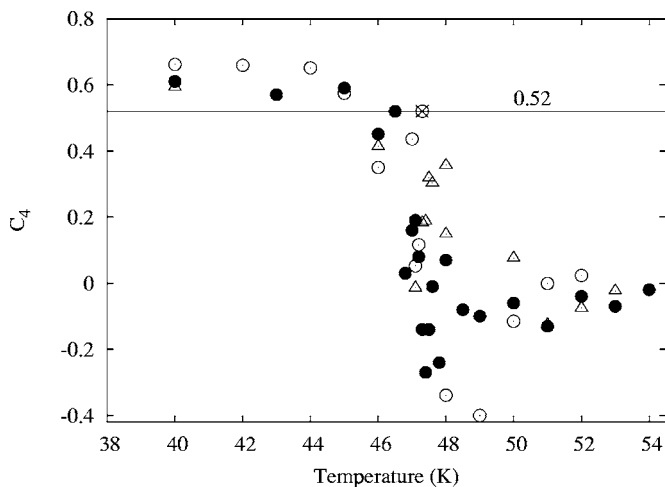


FIG. 9. The calculated fourth cumulant versus temperature. The open circles, closed circles, and the triangles represent $\rho=0.39$, 0.71, and 1.00, respectively.

adlayer interaction embodied by E_1 . This view will be expanded upon later.

At densities $1.07 \leq \rho \leq 1.31$, the calculated orientational character of the system is different. In this range there is no evidence of the sharp peak in the calculated specific heat. This is in accord with experiment.² At $\rho=1.07$, the orientational probability distribution showed only a single, sharp peak at $\Theta = \pm 2.8^\circ$ for temperatures $T \leq 45$ K. At higher temperatures and until melting at $T_m=51$ K, the orientational probability distribution is fairly flat between seven and minus seven degrees. There are small peaks at 0° , $\pm 2.8^\circ$, and $\pm 7^\circ$. Unlike at lower densities, there is no dominant peak at zero degrees below melting. Instead, the orientational character of the adlayer in the region $45 \text{ K} < T < T_m$ is more like a system in which there is no stable orientation; it is orientationally disordered. The many local minima in the potential are too weak to do other than modulate the disorder. We conclude that there is no transition from an angle of 2.8° to one along a substrate symmetry axis until melting.

The calculated orientational behavior for $\rho=(1.14, 1.22)$ is qualitatively the same as described above for 1.07. The rotational angle was at about 2.9° for all temperatures up to about 5 K of melting, as indicated by a sharp peak in the orientational probability distribution. Upon increasing the temperature toward T_m , multiple peaks in the probability distribution appear. The peaks are not much higher than the background probability which extends between $\pm 15^\circ$. Again, the adlayer seems to evolve from a distinct orientation with respect to the substrate to a relatively orientationally disordered state around 5 K below T_m and that persists until melting. Note that $T_m=(70 \text{ K}, 74 \text{ K})$ for $\rho=(1.14, 1.22)$. An adlayer with a surface density of 1.31 behaves differently than those at lower densities. It is found that the adlayer is oriented along a substrate symmetry axis at low temperatures and that persists until 60 K. The next calculated data point is at 70 K, where the adlayer has rotated to an angle of $\Theta = 2.7^\circ$. This orientation persists until melting at 77 K. There is no explanation of this behavior but some aspects of it will be presented in Sec. IV.

C. Lattice parameters

The lattice parameters are determined by taking the Fourier transform of the calculated pair distribution function. It shows peaks at reciprocal lattice vectors \vec{k} associated with the triangular argon adlayer. One peak is at $\vec{k} = (0, 4\pi/a\sqrt{3})$, from which the lattice constant is determined, i.e., $a = 4\pi/k\sqrt{3}$.

Calculating lattice parameters for partial monolayers at low surface densities are difficult because size effects can compromise the accuracy of the results. At low densities the Ar atoms do not cover the entire surface of the MC cell. At low temperature they form a 2D cluster that maximizes the coordination number of the atoms and minimizes the internal energy. This situation depreciates the use of periodic boundary conditions to simulate a physical system. For example, suppose the number of particles used in the MC cell is $N = 256$, which was generally used in this work. Then the cluster in the MC cell is remote from equivalent clusters in

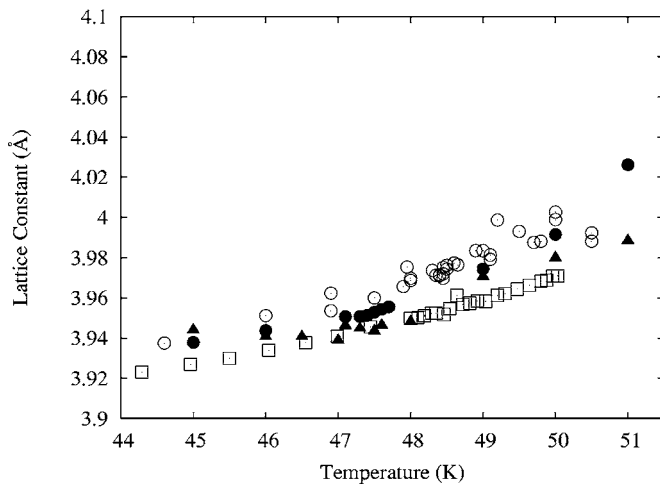


FIG. 10. The solid inverted triangle and the solid circle give the calculated lattice parameters for $\rho=0.39, 0.71$, respectively. The size effect correction discussed in the text is applied to the results for $\rho=0.71$. For $\rho=0.39$, $N=624$ was used. The open diamonds give the experimental results of Shaw *et al.* (Ref. 8) and the open square gives the experimental results of D'Amico *et al.* (Ref. 7)

nearby periodic cells and it is, therefore, nearly isolated. It follows that about 25% of the Ar atoms are on the edge of the cluster and they have a different environment than those inside. This is quite different from clusters examined experimentally at the same surface density. They are macroscopic in size and the difference is important in calculations of the lattice parameters where errors of fractions of one percent are significant. This problem is solved here by increasing the number of particles examined in the MC cell. A calculation of the lattice parameters for an adlayer with $\rho=0.7$ was done for many different numbers of particles from $N=144$ to 1024. The results showed that the calculated lattice parameter drops rapidly from $N=144$ until $N=324$, and beyond that, it remains nearly constant. The size effect from $N=256$ to 324 was more than 1%. This study of size effects is essentially temperature independent.

To solve the problem, lattice parameters at $\rho=0.39$ were calculated with $N=625$ and for $\rho=0.71$, they were calculated with $N=256$ and the size effect correction described above was used. The results are shown in Fig. 10 including all experimental data.^{6,7} Comparison between theory and experiment is satisfactory. The slope of the calculated lattice parameters change abruptly at $T=47.4$ K, which is also the calculated temperature for the orientational transition. At $\rho=1.00$, the calculated lattice parameter increases about 5% between 45 K and 51 K. Note that lower limit of this interval is just below the temperature of the rotational transition and the higher limit is that of melting. Beyond melting, the lattice constant is nearly constant at ≈ 4.1 Å until $T=70$ K, the highest calculated temperature. This latest feature is understood by recognizing that the adlayer covers the entire substrate at higher temperatures where the Helmholtz free energy is minimized by the larger entropy of the more disordered adlayer. This characterization is confirmed by examining plots of the adatoms position. Then the adlayer cannot easily thermally expand in the substrate plane, and the

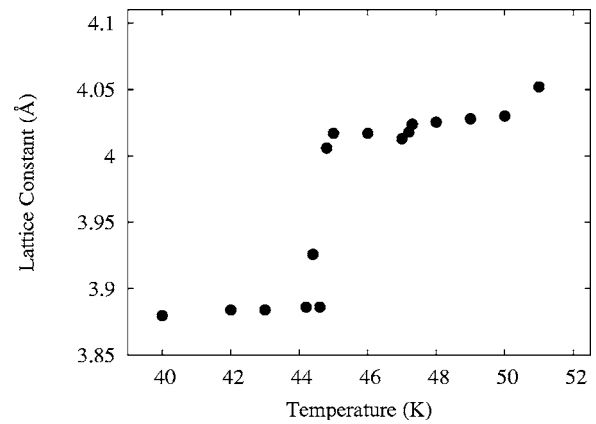


FIG. 11. The calculated lattice parameter for $\rho=1.07$.

lattice constant is nearly independent of temperature. This situation persists until the second layer promotion is thermally activated.

Figure 11 shows the calculated lattice parameter for $\rho=1.07$ with $N=256$. Size corrections were not applied because, at that density, the substrate is nearly covered and the periodic boundary conditions effectively reduce size effects. We estimate the maximum uncertainty due to the effect is less than 0.25%. The figure is similar to the one for $\rho=1.00$, but the change at 44 K is extremely abrupt and well below melting, which occurs at 51 K. The calculated specific heat at $\rho=1.07$, shown in Fig. 3, fluctuates considerably at the temperature of the jump in the lattice constant. This jump occurs some 3 K below the temperature of the rotational transition seen at lower densities. But no such transition is seen at $\rho=1.07$.

A general understanding of the transitions in this system is elucidated by using the strategy of Novaco and McTague.⁴⁰ The part of the adlayer-substrate potential that is responsible for its variation across the substrate is E_1 and it is viewed as applying a stress on the adlayer. As the temperature increases the stress may increase and at some temperature the stress is relieved in some way. There are several ways the stress can be relieved; a rotational transition, a change in the lattice parameter, by second layer promotion, or any combination of the above. The results presented above show that, at low surface densities, the stress is relieved by a rotational transition accompanied by a change in the lattice parameters. The change in the lattice parameters at this transition preempts the change usually occurring at melting.

Figure 12 shows the calculated lattice parameters for $\rho=1.14, 1.22$, and 1.31. With $N=256$, no size correction is required because the boundary conditions adequately simulate a macroscopic system. Note that the density of a complete monolayer is $\rho \approx 1.25$. It is apparent that the coefficient of thermal expansion for all three densities change greatly at 3–4 K below melting despite any evidence of a rotational transition, except for $\rho=1.31$, which seems to exhibit a rotation at 70 K. The character of thermal expansion is complicated at these densities because significant second layer promotion occurs at temperatures $T \geq 65$ K, which depletes the monolayer. Features of this phenomena are described below.

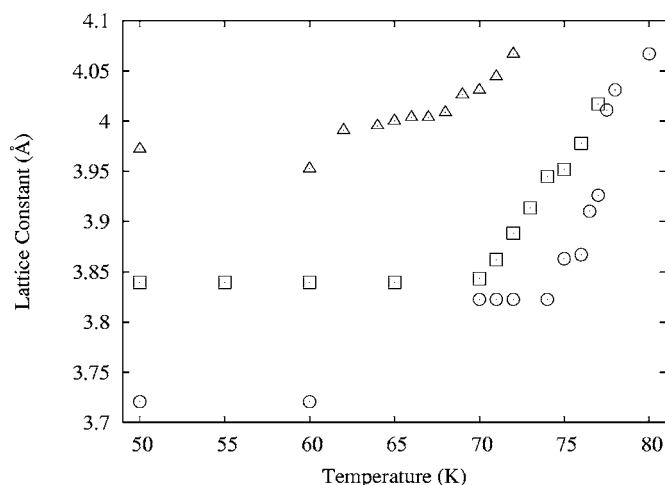


FIG. 12. The crosses, squares, and circles show the calculated lattice parameters for $\rho=1.14$, 1.22, and 1.31, respectively.

D. The other dimension

The behavior of adlayers is often examined by concentrating on dynamics in the (x,y) plane of the substrate, and contributions from motion in the normal direction is neglected. This strategy makes some sense when the normal holding forces are much stronger than forces between adatoms in the (x,y) plane, as is the case for the Ar/Gr systems. However, it will be shown that there are thermodynamic conditions where this approximation is very wrong.

Table I shows the melting temperature calculated in two different ways and at four different surface densities. The first column shows results where the z coordinates of all adatoms are treated as N independent degrees of freedom. The second column shows results where all z adatom coordinates were constrained to be fixed at the same equilibrium average value $\langle z \rangle$. For $\rho=0.71$, the table shows that the calculated value of T_m is unchanged by constraining the normal coordinates. This result is obtained at all calculated densities $\rho \leq 1.07$ as well. At higher densities, the table shows that use of the constraint greatly increases T_m . This general behavior was found earlier³⁸ in N_2/Gr , and the explanation given then is apparently general and is therefore valid for Ar/Gr. The argument is as following. At low surface densities the adlayer occupies only a part of the substrate. At low temperature the adatoms form a single, large cluster. At higher temperatures, they distribute more uniformly with many voids

TABLE I. The calculated melting temperatures at four different densities. The first column give results where all N adatoms z position are treated as independent degrees of freedom. The second column shows T_m when z is fixed.

Density	T_m	$T_m z$ fixed
0.71	49 K	49 K
1.14	70 K	85 K
1.22	74 K	92 K
1.31	77 K	240 K

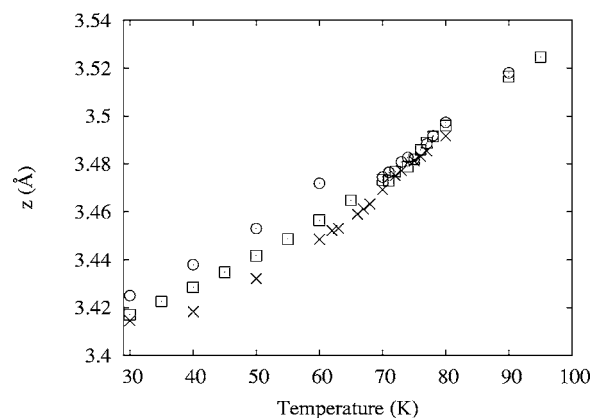


FIG. 13. The average calculated z position of the first layer versus temperature. The crosses, squares, and circles are for $\rho = 1.14$, 1.22, and 1.31, respectively.

and vacancies across the substrate. In both cases, there is considerable phase space in the (x,y) plane that is accessible to the adatoms; that facilitates 2D self-diffusion and a low melting temperature. With increasing density, 2D self-diffusion is more restricted and the thermal energy required to induce melting is greater, thus the melting temperature increases. An examination for Fig. 7 shows that this occurs for $\rho > 1.07$. This also is the density beyond which second layer promotion appears below melting. The promoted atoms reduce the surface density on the monolayer which enhances 2D self-diffusion, reducing the melting temperature. Thus, there are two competing phenomena that determine T_m at high densities. Since the second column in Table I show calculations that prevent second layer promotion, the results measure the relative importance of second layer promotion on reducing the melting temperature. Details about second layer promotion follows.

The most direct evidence for second layer promotion is from the calculated probability distribution for the z positions for the N atoms. At low temperatures, for all densities, a single sharp peak occurs at $z \approx 3.4$ Å. Figure 13 shows the average z position of the atoms in the first layer versus temperature at $\rho=1.14$, 1.22, and 1.31. The thermal expansion of $\langle z \rangle$ is apparent. For $\rho \geq 1.07$ and higher, a second peak in the probability distribution appears that signals that a second layer is forming. For $\rho=1.07$, second layer promotion begins at about 60 K, about 10 K above melting. Thus, it does not influence melting. For $\rho=1.14$, 1.22, and 1.31, the second layers begin between 60 to 70 K which is below melting. As discussed in the last paragraph, this dynamic has a profound effect on the melting temperature. The lattice parameters are also influenced by second layer promotion, shown in Fig. 12 for $\rho=1.14$, 1.22, and 1.31. These are for Ar atoms in the plane of the substrate. Note that for each density, the thermal expansion coefficient increases greatly at temperatures 3–4 K below melting and where second layer promotion starts. For the above mentioned densities, the height of the second layer is $\langle z \rangle = 6.5$ Å and there is no thermal expansion over the calculated interval $60 \leq T \leq 90$ K. Figure 14 shows the part of ρ that remains on the monolayer after second layer promotion occurs.

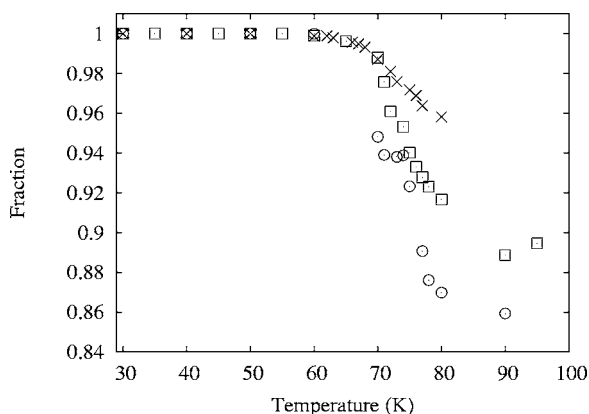


FIG. 14. The fraction of the total number of adatoms in the first layer versus temperature. The crosses, squares, and circles are for $\rho=(1.14, 1.22, 1.31)$, respectively.

IV. DISCUSSION AND CONCLUSIONS

An important result found from this calculation is the observation that melting is associated with the broad peak in the specific heat and that it seems to be continuous. This identification comes from the calculated order parameter that shows the loss of sixfold symmetry in the adlayer, from the pair distribution function, and from the configurations that become very disordered at temperatures beyond the transition. These results are in accord with findings from previous scattering experiments.³⁻⁷ Thus, the accumulated evidence is that the Ar/Gr system is the first documented case for melting that is not first order. The above discussion relates only to partial monolayers and there is little experimental information at higher densities near and above complete monolayer values. Our specific heat calculations at $\rho=1.31$ shows that the melting peak is much sharper than at lower densities; see Fig. 3. It could be speculated that melting may become first order at even higher densities but there is no information to test this idea. The calculated melting curve, shown in Fig. 7, follows the experimental data^{1,2} quite well and the slope changes drastically at $\rho \approx 1.07$. There is a conjunction of several events at that density; the rotational transition disappears, self-diffusion in the (x, y) plane becomes significantly inhibited by the increased numbers of adatoms, and thermally activated second layer promotion occurs near melting. The calculations summarized in Table I reveal that motion of adatoms in the z direction is an important aspect of melting. For $\rho \leq 1.07$, the calculated melting temperature is unchanged by applying the constraint which forbids motion in the normal direction. However, for $\rho > 1.07$, the constraint dramatically increases the predicted melting temperature. It is apparent that depletion of the monolayer by second layer promotion increases self-diffusion and acts to lower the melting temperature. As expected, the effect is bigger at higher densities. This depletion is prevented when the constraint is applied.

The character of the sharp specific heat peak was determined by calculating the probability distribution of all nearest neighbor Ar-Ar bond angles with respect to a sixfold symmetry axis of the substrate. For densities $\rho \leq 1.00$ the

orientational angle was approximately constant until 47.4 K, and it changes to zero over an interval of $\Delta T=0.3$ K, as seen in Fig. 8. This is precisely the temperature and the width of the sharp specific heat peak. Moreover, the fourth cumulant of the rotational angle has the signature of an orientational transition at the same temperature. The character of the sharp peak is apparently rotational. For the calculated densities $1.07 \leq \rho \leq 1.31$, the sharp specific heat peak disappears; as seen in Fig. 3. The calculated rotational angles for $\rho=1.07$, 1.14, and 1.22 show no transition either. Instead, they are rotated by about 2.8° until the temperature rises to within a few degrees of melting. Then the probability distribution shows multiple small peaks that are just resolved above a flat background between $-15^\circ \leq \Theta \leq +15^\circ$. There is no dominant peak at zero degrees until melting, and there is no sign of a transition of the adlayer to an angle along a substrate symmetry axis. This conclusion is consistent with the lack of a rotational peak in the calculated specific heats at these densities, and by experiment.² By examining the evolution of the configurations along the MC sequence near melting, we conclude that the orientations seem disordered with a small modulation due to weak local minima in the potential. Different initial conditions were used and many more steps were added to ensure that the thermal averages of physical quantities are in equilibrium. The results were always the same. The orientational character of the adlayer is different for $\rho=1.31$, about 5% greater than monolayer completion. At low temperatures, the adlayer orients along a substrate symmetry axis. At about 70 K, it makes a transition to a rotational angle of 2.7° which persists until melting at 77 K. The lattice parameters shown in Fig. 12 indicate a transition although too few points in the range between 60 to 80 K were calculated to precisely resolve it. Despite that problem a tentative explanation of the adlayer behavior at $\rho=1.31$ is possible. At low temperatures the adatoms are all in the monolayer plane. Results show that at monolayer and higher densities the adlayer forms a triangular lattice that orients along a substrate symmetry axis. However, for $\rho=1.31$ at 70 K, Fig. 14 shows that about 7% of the adatoms are in the second layer. This means that the effective density of the monolayer is close to 1.22 at 70 K. Our results for the orientational angle for $\rho=1.22$ at low temperature is the same as for $\rho=1.31$ at 70 K. It is apparent that the interpretation of the results is more complicated at densities and temperature where second layer promotion is significant.

The calculated lattice parameters at partial monolayer densities, shown in Fig. 10, underscore the importance of reducing possible size effects. In this case, thermal averages must be calculated within an uncertainty of much less than one percent accuracy to ensure reliable results for adlayer thermal expansion. As previously discussed, size effects are particularly big at low surface densities and temperatures where the periodic boundary conditions do not simulate a macroscopic physical sample very well. Another feature that complicates the interpretation of lattice parameter behavior is second layer promotion. The fraction of adatoms in the second layer is almost entirely due to thermal excitation that begins at about 60 K. As Fig. 13 shows, the behavior of the lattice parameters are sensitive to those excitations.

Despite the good connection this work makes with experiment, there is one feature that is not resolved. The calculated

sharp peak in the specific heat is clearly identified as due to a rotational transition which occurs over a temperature interval of about 0.3 K. It is reasonable to assume that the rotation to an angle along the substrate symmetry axis occurs over that same interval. The calculation of the rotational angle versus temperature confirmed that assumption as shown in Fig. 8. However, the x-ray scattering experiment⁷ at $\rho=0.81$ shows that Θ continuously and monotonically decreases from 2.8° at about five degrees below melting, to 2° at melting and beyond. We are not able to explain this difference, but there are some possibilities. The experiment of Ma *et al.*³ showed that small concentrations of impurities in argon made big changes in the sharp specific heat peak, including its disappearance. The substrate used in the calculation is perfect, but real substrates used in experiment are not. Imperfections not present in the calculation could pin the adlayer and alter results. As for the calculation, the uncertainty in the strength of the adlayer-substrate part of the potential, discussed earlier, could be a problem. However, the good comparison between experiment and calculation for

other orientational properties makes this a remote source of the problem. Another feature of our results that needs additional study, is the orientational behavior of high density adlayers near melting. This study will be necessary to further refine this behavior. Finally, it is important to extend this work over a range of densities from one to two adlayers. This would give a thermodynamic map in a region where the building of additional adlayers occur and would give insights into the evolution toward bulk behavior.

ACKNOWLEDGMENTS

We thank Moses Chan for helpful discussions and a copy of Migone's thesis. We are also grateful to Hak Taub, F. Hanson, and L. Bruch for many valuable discussions and suggestions. Bogdan Kuchta and Lucyna Firlej did several preliminary side calculations that provided useful clues. Finally, we thank the Colorado State University high energy group for giving a great amount of computer time.

-
- ¹T. T. Chang, Surf. Sci. **87**, 348 (1979).
²A. D. Migone, Z. R. Li, and M. H. W. Chan, Phys. Rev. Lett. **53**, 810 (1984).
³J. Ma, E. D. Carter, and H. B. Kleinberg, Phys. Rev. B **57**, 9270 (1998).
⁴H. Taub, K. Carneiro, J. K. Kjems, L. Passell, and J. P. McTague, Phys. Rev. B **16**, 4551 (1977).
⁵J. P. McTague, J. Als-Nielsen, J. Bohr, and M. Nielsen, Phys. Rev. B **25**, 7765 (1982).
⁶M. Nielsen, J. Als-Nielsen, J. Bohr, J. P. McTague, D. E. Moncton, and P. W. Stephens, Phys. Rev. B **35**, 1419 (1987).
⁷K. L. D'Amico, J. Bohr, D. E. Moncton, and D. Gibbs, Phys. Rev. B **41**, 4368 (1990).
⁸C. G. Shaw, S. C. Fain, and M. D. Chinn, Phys. Rev. Lett. **41**, 955 (1978).
⁹M. Kosterlitz and D. J. Thouless, J. Phys. C **6**, 1181 (1973); B. I. Halperin and D. R. Nelson, Phys. Rev. Lett. **41**, 121 (1978); B. Halperin and D. Nelson, *ibid.* **41**, 519 (1978); D. R. Nelson and B. I. Halperin, Phys. Rev. B **19**, 2457 (1979); A. P. Young, *ibid.* **19**, 1855 (1979).
¹⁰P. A. Heiney, R. J. Birgeneau, G. S. Brown, P. M. Horn, D. E. Moncton, and P. W. Stephens, Phys. Rev. Lett. **48**, 104 (1982).
¹¹J. A. Litzinger and G. A. Stewart, in *Ordering in Two Dimensions* (North Holland, Amsterdam, 1980).
¹²A. J. Jin, M. R. Bjurstrom, and M. H. W. Chan, Phys. Rev. Lett. **62**, 1372 (1989).
¹³M. H. W. Chan, A. D. Migone, K. D. Miner, and Z. R. Li, Phys. Rev. B **30**, 2681 (1984).
¹⁴T. F. Rosenbaum, S. E. Nagler, P. M. Horn, and R. Clarke, Phys. Rev. Lett. **50**, 1791 (1983).
¹⁵D. Frenkel and J. P. McTague, Phys. Rev. Lett. **42**, 1632 (1979).
¹⁶S. Toxvaerd, Phys. Rev. Lett. **44**, 1002 (1980).
¹⁷D. Henerson, J. A. Barker, and F. F. Abraham, Physica A **106**, 226 (1981).
¹⁸L. W. Bruch, J. M. Phillips, and R. D. Murphy, J. Chem. Phys. **75**, 5097 (1981).
¹⁹J. Q. Broughton, G. H. Gilmer, and J. D. Weeks, Phys. Rev. B **25**, 4651 (1982).
²⁰C. Udink and J. van der Elksen, Phys. Rev. B **35**, 279 (1987).
²¹A. F. Bakker, C. Bruin, and H. J. Hilhorst, Phys. Rev. Lett. **52**, 449 (1984).
²²K. J. Strandburg, J. A. Zollweg, and G. V. Chester, Phys. Rev. B **30**, 2755 (1984).
²³P. D. Frenkel, M. P. Allen, and W. Gignac, J. Chem. Phys. **78**, 4206 (1983).
²⁴A. D. Novaco and P. A. Shea, Phys. Rev. B **26**, 284 (1982).
²⁵M. W. Roth and M. Salazar, Surf. Sci. **441**, 270 (1999).
²⁶F. F. Abraham, Phys. Rev. B **29**, 2606 (1984); **28**, 7338 (1983).
²⁷F. F. Abraham, Phys. Rev. Lett. **44**, 463 (1980).
²⁸R. D. Eters, E. Flenner, B. Kuchta, L. Firlej, and W. Przydrozny, J. Low Temp. Phys. **122**, 121 (2001).
²⁹E. Flenner and R. D. Eters, Phys. Rev. Lett. **88**, 106101 (2002).
³⁰R. Aziz and M. Slaman, J. Chem. Phys. **92**, 1030 (1990).
³¹B. M. Axilrod and E. Teller, J. Chem. Phys. **11**, 229 (1943).
³²A. McLachlan, Mol. Phys. **7**, 381 (1964).
³³L. Bruch, Surf. Sci. **36**, 317 (1973).
³⁴W. Carlos and M. Cole, Surf. Sci. **91**, 339 (1980).
³⁵W. Steele, Surf. Sci. **36**, 317 (1973).
³⁶(private Communication).
³⁷H. Taub, K. Carneiro, J. K. Kjems, L. Passell, and J. P. McTague, Phys. Rev. B **16**, 4551 (1977).
³⁸B. Kuchta and R. D. Eters, Phys. Rev. B **54**, 12057 (1996).
³⁹K. Binder, Phys. Rev. Lett. **47**, 693 (1981).
⁴⁰A. D. Novaco and J. P. McTague, Phys. Rev. Lett. **38**, 1286 (1977).